Check for updates

ADVANCED QUANTUM TECHNOLOGIES
www.advquantumtech.com

Spin Pumping in Epitaxial $Ge_{1-x}Sn_x$ Alloys

Emanuele Longo, Omar Concepción, Roberto Mantovan, Marco Fanciulli, Maksym Myronov, Emiliano Bonera, Jacopo Pedrini, Dan Buca, and Fabio Pezzoli**

The use of $Ge_{1-x}Sn_x$ semiconductor alloys is generating significant interest in the scientific community due to their precisely tunable Sn content. This tunability makes them particularly attractive for applications in photonics, electronics, and, more recently, spintronics. Room-temperature emission and detection of spin currents are observed in $Ge_{1-x}Sn_x$/Co hybrids through spin-pumping ferromagnetic resonance. Experiments conducted over a wide range of compositions and strains show that spin current injection is enhanced in $Ge_{1-x}Sn_x$ solid solutions compared to elemental Ge. The magnetization dynamics reveal an intriguing scenario where the Gilbert damping constant and the spin mixing conductance display a non-monotonic behavior. The maximum spin-pumping efficiency occurs at a Sn molar fraction of ≈10 at.% and remains unaffected by the elastic strain built up in $Ge_{1-x}Sn_x$ films through epitaxial growth on Ge-buffered Si substrates. These findings highlight the non-trivial dependence of alloy scattering in defining spin accumulation and relaxation mechanisms, providing insightful information on phenomena at the forefront of spintronics and quantum technology research.

1. Introduction

The development of fast and energy-efficient electronic devices is crucial to overcoming the challenges of information and communication technologies (i.e., big-data storage and processing).[1] Spintronic devices exploit the spin dynamics to engineer new functionalities, thereby offering promising solutions to move beyond the more-than-Moore scenario. In this context, the mutual interconversion between spin and charge currents represents a tantalizing approach. In particular, when high spin-orbit coupling (SOC) materials (i.e., heavy metals) are placed in contact with ferromagnets (FMs), the magnetization can be manipulated through the so-called spin Hall effect (SHE). Here, a charge current flowing inside a non-magnetic material (NM) is converted into a pure spin current and subsequently injected into the adjacent FM. The efficiency of the spin-to-charge conversion (SCC), hence the generated spin current, is directly connected to the strength of the SOC in the NM.[2] Recently, the SCC studies have been extended to microelectronic compatible semiconductors, e.g., group IV materials like Si and Ge,[3,4] to exploit their notable spin diffusion length.[5–10] The SOC present in elemental Si and Ge can be further enhanced by the incorporation of Sn into the lattice. These new GeSn semiconductor alloys have recently aroused great interest in the scientific community, given the tunability of the alloy's bandgap as a function of Sn, resulting in attractive properties to be exploited in photonics, electronics, and recently in spintronics.[5,11,12]

In this work, the spin pumping (SP) mechanism in GeSn alloys is investigated. The alloy stoichiometry and lattice strain are used to control the strength of the spin-orbit coupling, and its influence on the spin momentum accumulation. To this aim, room temperature (RT) experiments relying on SP ferromagnetic resonance (SP-FMR) are performed over a broad frequency range.

The non-magnetic (NM) semiconductor GeSn/Ge/Si(100) epitaxial growth is performed on 200 mm wafers by chemical vapour deposition (CVD) method using standard Si technology reactors.[13,14] Two sets of samples of similar Sn atomic content were grown, with the aim of studying the strain effect by varying the Sn fraction and by considering the two thicknesses of 40 nm and 400 nm. The 40 nm GeSn samples are lattice-matched with the Ge buffer, and they are highly compressively strained with the strain determined by the Sn content. On the other hand, the 400 nm GeSn samples are highly strain-relaxed. In both cases,

E. Longo
Institute of Materials Science of Barcelona (ICMAB-CSIC)
Campus de la UAB
Bellaterra 08193, Spain
E-mail: elongo@icmab.es

E. Longo, R. Mantovan
CNR-IMM
Unit of Agrate Brianza (MB)
Via C. Olivetti 2, Agrate Brianza 20864, Italy

O. Concepción, D. Buca
Peter Gruenberg Institute 9 (PGI 9) and JARA-Fundamentals of Future Information Technologies
Forschungszentrum Juelich
52428 Juelich, Germany

M. Fanciulli, E. Bonera, J. Pedrini, F. Pezzoli
Dip. di Scienza dei Materiali
Università degli studi di Milano-Bicocca and BiQuTe Via R. Cozzi 55
Milano 20126, Italy
E-mail: fabio.pezzoli@unimib.it

M. Myronov
Department of Physics
The University of Warwick
Coventry CV4 7AL, UK

The ORCID identification number(s) for the author(s) of this article can be found under https://doi.org/10.1002/qute.202400508

© 2024 The Author(s). Advanced Quantum Technologies published by Wiley-VCH GmbH. This is an open access article under the terms of the Creative Commons Attribution License, which permits use, distribution and reproduction in any medium, provided the original work is properly cited.

DOI: 10.1002/qute.202400508

Table 1. Summary of the stack and properties of the samples studied.

Label	Stack	Sn at.%	$g^{eff}_{\uparrow\downarrow} \cdot 10^{19} (m^{-2})$
$Ge_{1-x}Sn_x$(40)	Au/Co/Au/Ge/Si	0	
	Au/Co/Au/40 nm Ge_xSn_y/Ge/Si	3	2.47 ± 0.75
		6	3.26 ± 0.77
		10	3.98 ± 0.85
		11	4.13 ± 0.90
		12	2.32 ± 0.76
		13	1.40 ± 0.80
$Ge_{1-x}Sn_x$(400)	Au/Co/Ge/Si	0	
	Au/Co/400 nm Ge_xSn_y/Ge/Si	4	1.31 ± 0.17
		8	2.36 ± 0.20
		10	3.74 ± 0.22
		12	1.67 ± 0.20
		14	1.22 ± 0.19

the Sn content varies between 0 and 13 at.%. The full samples' description is reported in **Table 1**. As detailed in the next section, an unexpected non-monotonic dependence of the Sn content is observed, which is attributed to the non-trivial role of $Ge_{1-x}Sn_x$ alloys as a sink for the spin current.

Spin pumping in $Ge_{1-x}Sn_x$ alloys appears to play a central role in establishing a better understanding of the implications of strain and band-gap engineering in spin accumulation processes. Therefore, such investigations are expected to be useful in assessing the potential integration of spin-augmented functionalities into state-of-the-art semiconductor technologies. More generally, the control over the spin flow and SOC-induced phenomena, particularly in group IV materials, opens novel and exciting perspectives in the emerging fields of spin-orbitronics and quantum electronics.

2. Results and Discussion

Figure 1a,b depicts the X-ray diffraction reciprocal space maps (XRD-RSM) of GeSn layers of 10 at.% Sn content with a thickness of 40 and 400 nm respectively, to judge the thickness-dependence of the lattice strain. Notably, the position of the GeSn (40 nm) XRD-RSM peak relative to the Ge substrate confirms that the epilayer is fully strained, with no indication of a relaxed component.

The uniform Sn distribution in the layers is provided by the atom probe tomography (APT) data (Figure 1c) and the secondary ion mass spectrometry (SIMS) line profile along the layer depth (Figure 1d). The high crystalline quality of the epitaxial GeSn layers is illustrated through a high-resolution transmission electron microscope (HR-TEM) image in Figure 1e. For spin-pumping measurements, the FM stack differs for the two GeSn sets. For the pseudomorph $Ge_{1-x}Sn_x$(40) set, it consist of 5 nm Au/ 10 nm Co/ 5 nm Au, as deposited on GeSn. The presence of an Au interlayer decouples the $Ge_{1-x}Sn_x$ and Co layers inhibiting exchange coupling arising from the orbital hybridization at the FM/NM heterojunction. This makes $Ge_{1-x}Sn_x$ a suitable platform to study the Sn-induced influence on the SCC mechanisms.

The FM stack for the strain-relaxed GeSn set of samples is prepared to further examine the potential interplay between the strain and SOC. In this case, it consists only of a 5 nm Au/ 10 nm Co. The modification introduced to the FM stack compared to the $Ge_{1-x}Sn_x$(40) set is further discussed later in the text. A schematic of the two sample sets is shown in Figure 1f,g.

The dynamic of the magnetization vector ($\vec{M}$) in a FM under an external magnetic field ($\vec{H}_{ext}$) is described by the Landau–Lifshitz–Gilbert equation, which consists of a precessional and a damping-like term:

$$\frac{d\vec{M}}{dt} = -\mu_0 \gamma \vec{M} \times \vec{H}_{ext} + \frac{\alpha}{M_s} \left(\vec{M} \times \frac{d\vec{M}}{dt} \right) \quad (1)$$

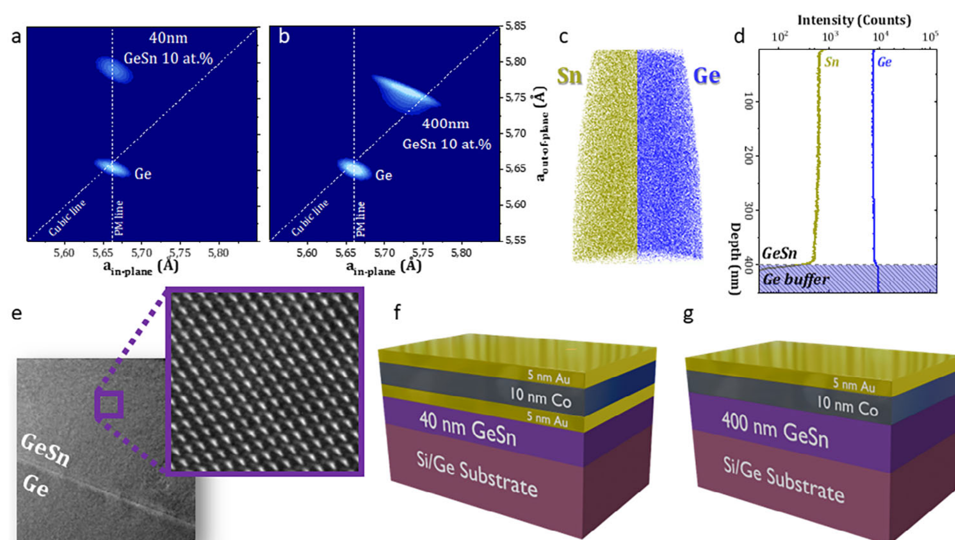

Figure 1. XRD-RSM of (a) a compressive-strained $Ge_{1-x}Sn_x$(40) and (b) an almost fully-relax $Ge_{1-x}Sn_x$(400) with a Sn content of 10 at.%. (c) APT reconstruction showing a uniform elemental atomic distribution of Ge and Sn and (d) SIMS profile through the full layer. (e) HR-TEM image showing a sharp interface between the $Ge_{1-x}Sn_x$ layer and the Ge buffer with an atomic zoom-in on the $Ge_{1-x}Sn_x$ crystal structure. (f,g) 3D sketch of the layers stacks for the SP-FMR measurements at RT.

© 2024 The Author(s). Advanced Quantum Technologies published by Wiley-VCH GmbH

25119044, 0, Downloaded from https://onlinelibrary.wiley.com/doi/10.1002/qute.202400508 by CochraneItalia, Wiley Online Library on [23/12/2024]. See the Terms and Conditions (https://onlinelibrary.wiley.com/terms-and-conditions) on Wiley Online Library for rules of use; OA articles are governed by the applicable Creative Commons License

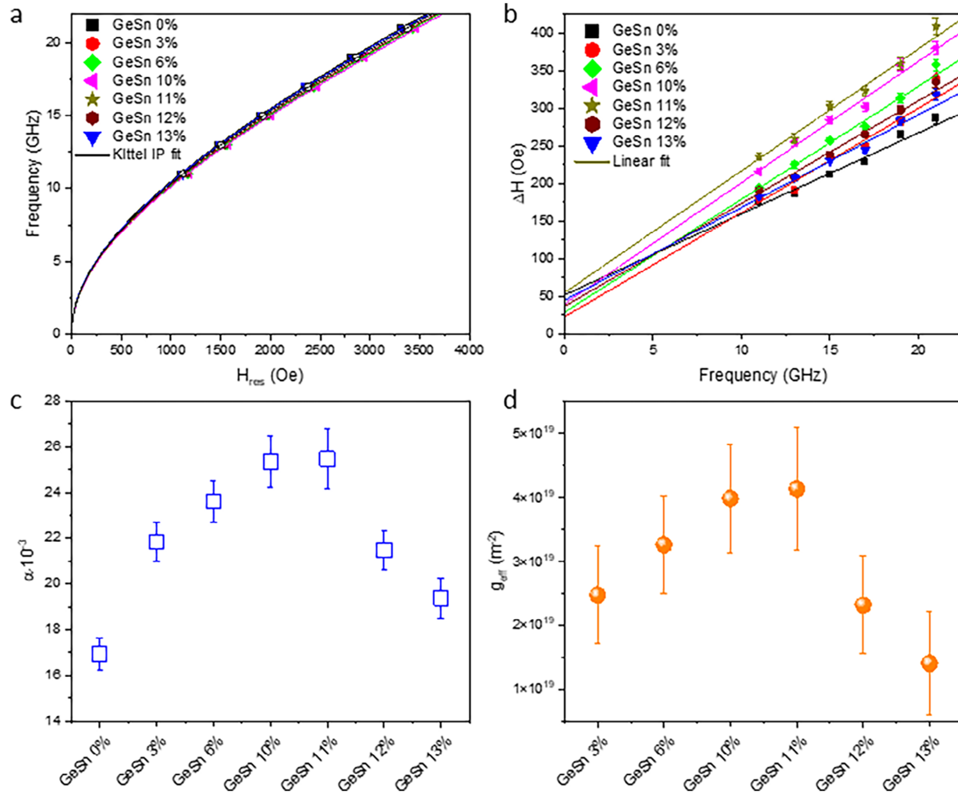

Figure 2. (a) Kittel curves describing the ferromagnetic resonance frequency f_{res} versus the resonance field H_{res} measured for the various Sn at.% of the $Ge_{1-x}Sn_x$(40) set. (b) Linewidth of the broad-band FMR resonance ΔH as a function of the microwave frequency. Panels (c,d) show the values of the damping constant, α, and the spin mixing conductance, $g_{\uparrow\downarrow}^{eff}$ obtained by using Equations (3) and (4), respectively.

where μ_0 is the Bohr magneton, $\gamma = g\frac{e}{2m_e}$ the gyromagnetic ratio with g the g-factor, e the charge of the electron, and m_e the effective free electron mass, M_s is the saturation magnetization, and α the damping constant. To extract quantitative information from the SP-FMR measurements,Au/Co/Au/Ge/Si(100) and Au/Co/Ge/Si(100) heterostructures are adopted as references for the $Ge_{1-x}Sn_x$(40) and $Ge_{1-x}Sn_x$(400) sets, respectively. The differential nature of the SP-FMR analysis further guarantees the minimization of spin-related parasitic effects occurring in the FM stack rather than in the $Ge_{1-x}Sn_x$ epitaxial layer.

Figure 2a displays the evolution of the Kittel curves acquired in the in-plane (IP) geometry (see Methods) for thin $Ge_{1-x}Sn_x$(40), which links the resonant frequency (f_{res}) with the resonant magnetic field (H_{res}).[15] For polycrystalline ferromagnetic thin films (i.e., no IP anisotropy), the Kittel equation assumes the following form:

$$f_{res} = \frac{\gamma}{2\pi}\sqrt{H_{res}\,\left(H_{res} + 4\pi M_{eff}\right)} \quad (2)$$

where M_{eff} represents the effective magnetization (i.e., for thin films $M_s \sim M_{eff}$). Since the Co layers are simultaneously deposited on all samples, we can reduce the number of free fitting parameters, keeping γ constant at $1.95 \cdot 10^7 \frac{Hz}{Oe}$, which corresponds to the Landé factor g = 2.25.[16,17] The M_{eff} values extracted from Figure 1a for pseudomorphic $Ge_{1-x}Sn_x$(40) samples show a clear Sn content dependence, with a minimum around Sn 10 at.% (see Figure S1a, Supporting Information). M_{eff} is directly connected to the presence of magnetic surface anisotropy (K_s) in the Co layer, and it is defined as $4\pi M_{eff} = 4\pi M_s - \frac{2K_s}{M_s t_{Co}}$, where M_s and t_{Co} are the saturation magnetization and the thickness of the Co layer, respectively.

The quality of NM/FM interfaces can affect the physics on the spin accumulation.[18] In particular, the emergence of a remarkable surface anisotropy contribution in Au/Co/Au heterostructures is a well-known effect that favors the out-of-plane magnetization of the Co interface atoms.[19,20] This anisotropy can be influenced by epitaxial strain in the Au layer, modified spin-orbit coupling interactions due to the hybridization of Au 5d and Co 3d orbitals, as well as chemical and morphological properties of the Au/Co interface (e.g., roughness and chemical intermixing).[21–24] In the present study, the epitaxial $Ge_{1-x}Sn_x$(40) series exhibits varying strain conditions as a function of Sn at.%. Moreover, the different Sn content modulates the SOC strength, influencing the orbital hybridization between Au and the $Ge_{1-x}Sn_x$ layers. This may affect the spin polarization and magnetic coupling at the Au/Co upper interface. These factors collectively modify the electronic structure of the $Ge_{1-x}Sn_x$(40) system, achieving a maximum K_s value at an optimal Sn concentration. Additionally, this intermediate Sn at.% can result in

© 2024 The Author(s). Advanced Quantum Technologies published by Wiley-VCH GmbH

25119044, 0, Downloaded from https://onlinelibrary.wiley.com/doi/10.1002/qute.202400508 by CochraneItalia, Wiley Online Library on [23/12/2024]. See the Terms and Conditions (https://onlinelibrary.wiley.com/terms-and-conditions) on Wiley Online Library for rules of use; OA articles are governed by the applicable Creative Commons License

a slightly smoother and higher-quality interface, minimizing defects and interdiffusion, which further enhances the anisotropic properties.

The linewidth (i.e., full width at half maximum) of the broadband FMR signal (ΔH) as a function of f_{res} is shown in Figure 2b. The solid lines indicate the modelling of the data based on the following equation:

$$\Delta H = \Delta H_0 + \frac{4\pi}{|\gamma|} \alpha f_{res} \tag{3}$$

where ΔH_0 represents the inhomogeneous line broadening and provides information about the magneto-structural properties of the Co film (i.e., magnetic dead layers, structural defects, etc.). The ΔH_0 lies in the 25–50 Oe range for all the samples, confirming the good quality of the deposited FM films.[15,25,26]

In Figure 2c the dependence of α on the Sn content demonstrates a maximum for the $Ge_{0.89}Sn_{0.11}$(40) sample, suggesting a marked improvement of the SP efficiency compared to the case of the elemental, not-alloyed Ge reference.

To better understand this finding, we can consider that according to the SP theory,[15,27–29] the power loss described by α is directly proportional to the effective spin mixing conductance ($g_{eff}^{\uparrow\downarrow}$), which is defined as:

$$g_{eff}^{\uparrow\downarrow} = \frac{4\pi M_s t_{FM}}{g\mu_B} \left(\alpha_{FM/GeSn} - \alpha_{FM/Ge}\right) \tag{4}$$

with t_{FM} being the thickness of the FM layer, and in this case, $\alpha_{FM/GeSn}$ and $\alpha_{FM/Ge}$ are the damping constants of the $Ge_{1-x}Sn_x$(40) samples with and without Sn, respectively. The spin mixing conductance represents an intrinsic property of a SCC system, being proportional to the amount of the spin current injected across the FM/NM interface. The aim of this study is to highlight the role of Sn in $Ge_{1-x}Sn_x$. In the following, $g_{eff}^{\uparrow\downarrow}$ is thus extracted relatively to an elemental Ge reference. It should be noted that this approach provides an effective rather than absolute estimation of, which is known to be non-zero in Ge/FM heterostructures.[27] From a phenomenological point of view, when a spin current generator, that is, a FM, is in contact with a spin sink, i.e., the $Ge_{1-x}Sn_x$ film, the generated spin current can be pumped inside the NM layer depending on the $g_{eff}^{\uparrow\downarrow}$ value. The higher is $g_{\uparrow\downarrow}^{eff}$, the more transparent is an interface. Indeed, the spin current density (J_s^{3D}) generated in the system is defined as:

$$J_s^{3D} = \frac{\hbar}{4\pi} g_{eff}^{\uparrow\downarrow} \left[\vec{M} \times \frac{d\vec{M}}{dt}\right] \tag{5}$$

which is attributed to an imbalance of spins with opposite orientations in different regions of the FM.[15,28,29]

Figure 2d summarizes $g_{eff}^{\uparrow\downarrow}$ derived by Equation (4) using the Sn-free Au/Co/Au/Ge/Si(100) reference. The extracted values fall in the $1-4 \cdot 10^{19}\ m^{-2}$ range, thus comparing well with results obtained for state-of-the-art SCC materials (see Table 1 in the Supporting Information of ref.[30]). As expected, the $g_{eff}^{\uparrow\downarrow}$ maps out the behavior of α (Figure 1c), reaching a maximum at $Ge_{0.89}Sn_{0.11}$(40), and demonstrating a clear-cut enhancement by almost four times with respect to the minimum $g_{eff}^{\uparrow\downarrow}$ evaluated at the two boundaries of the composition range explored in this work. Moreover, to further assess the role in the spin transport process of the insertion of the Au layer between the FM and NM, a $Ge_{1-x}Sn_x$(40) Au interlayer-free sample with $x \sim 10$ at.% was grown, and the $g_{eff}^{\uparrow\downarrow}$ compared with the $Ge_{1-x}Sn_x$(40) sample having the same Sn at.% (see Figure S2, Supporting Information). As a result, no difference was observed, thus demonstrating that spin-dependent contributions from the metal interlayer can be safely ruled out. This is in agreement with the Au thickness being almost one order of magnitude smaller than the spin diffusion length.[25,31]

At first glance, the increasing Sn content in the $Ge_{1-x}Sn_x$(40) series can thus be correlated with the strengthening of the SOC, being larger than in Ge. Nevertheless, the non-linear response of $g_{eff}^{\uparrow\downarrow}$ suggests a more complex scenario, where competing effects are likely to occur and ultimately determine the peculiar SCC response observed in our SP-FMR experiments.

To better clarify these mechanisms we can start our discussion by considering that the $Ge_{1-x}Sn_x$(40) films are under compressive strain. The latter increases with the Sn molar fraction of the alloy, owing to the progressive enlargement of the lattice mismatch with the Ge-on-Si substrate.[32]

The intertwined role of strain and Sn content on the spin-dependent phenomena has been investigated by Tai et al. in a 2D hole gas generated at the $Ge/Ge_{1-x}Sn_x$ interface.[33] The authors suggested the emergence of a strain-induced suppression of the Rashba SOC strength, stemming from the increase from 6 to 9–11 at.% of the Sn content when the $Ge_{1-x}Sn_x$ well is coherently grown on Ge-on-Si substrates. Qualitatively, the $g_{eff}^{\uparrow\downarrow}$ data reported in Figure 2d for the $Ge_{1-x}Sn_x$(40) suggests a very similar behavior, despite metallic-like Rashba states being inhibited in our case by the presence of the Au interposer. We can also find reassurance that interface states are indeed dummies by the measurement of the interlayer-free sample with $x \sim 10$ at.%(see Figure S2, Supporting Information).

Consequently, we can expect that when x is increased up to a critical value of $x_c \sim 10$ *at.%*, the magnetization dynamics losses in SP-FMR are mostly driven by the spin current channeled into $Ge_{1-x}Sn_x$ being a SOC-aided sink. In a virtual crystal approximation, the SOC scales indeed as Z_{eff}^4, where Z_{eff} is the effective atomic number of the binary alloy. Whereas above x_c, SOC turns out to be outsized by parasitic mechanisms, which effectively induce spin accumulation and reduce the damping process through the NM layer. In light of this phenomenological, albeit notable, analogy with ref.[33] it is therefore tempting to attribute to strain the behavior shown in Figure 2c,d, where a decrease of α and $g_{eff}^{\uparrow\downarrow}$ occurs in the high Sn range, i.e., at large strain values.

It should be noted, however, that the results obtained for the $Ge_{1-x}Sn_x$(40) set must be complemented by an independent analysis in order to fully elucidate the role of strain in shaping the non-trivial behavior of $g_{eff}^{\uparrow\downarrow}$.[33–35] To this purpose, we produced an separate set of fully-relaxed samples by growing the $Ge_{1-x}Sn_x$ epilayers with an increased thickness, while keeping fixed the spanned range of the Sn molar fractions. In addition, a simple Co(10 nm) layer is directly deposited on top of the $Ge_{1-x}Sn_x$-relaxed NM stack given the negligible spin resistivity through Rashba-like interface states (Figure S2, Supporting Information).

Following the same methodology used for the thinner $Ge_{1-x}Sn_x$(40) samples, we summarize in **Figure** 3a,b the Kittel

© 2024 The Author(s). Advanced Quantum Technologies published by Wiley-VCH GmbH

25119044, 0, Downloaded from https://onlinelibrary.wiley.com/doi/10.1002/qute.202400508 by CochraneItalia, Wiley Online Library on [23/12/2024]. See the Terms and Conditions (https://onlinelibrary.wiley.com/terms-and-conditions) on Wiley Online Library for rules of use; OA articles are governed by the applicable Creative Commons License

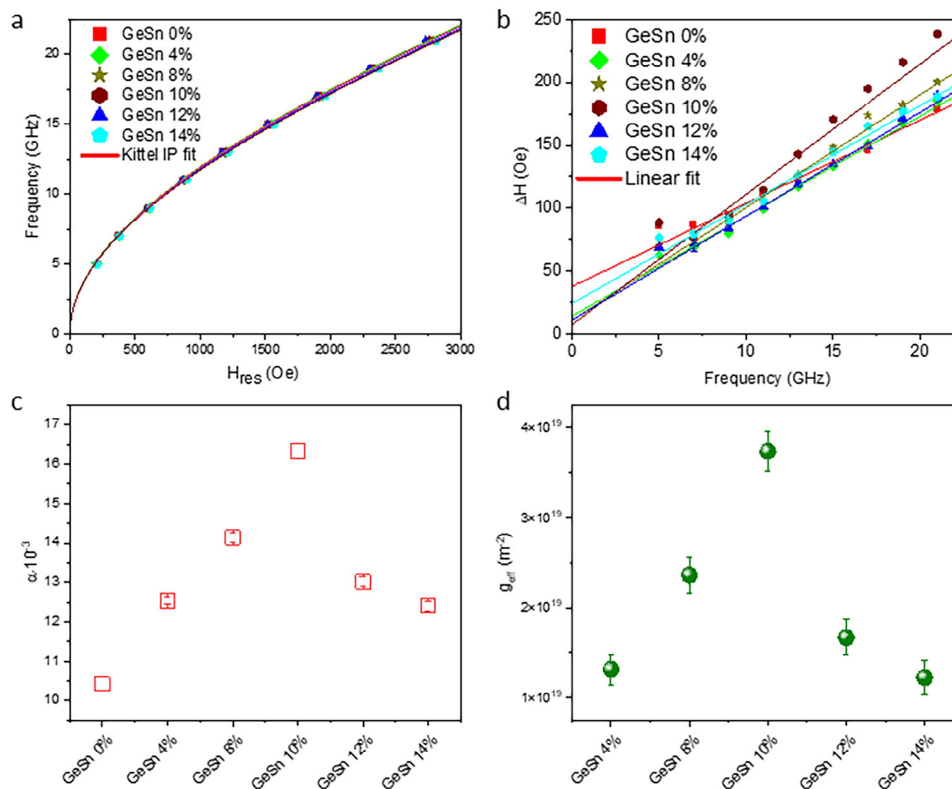

Figure 3. (a) Kittel curves describing the FMR frequency versus the resonance field H_{res} measured for the various Sn molar fraction of the $Ge_{1-x}Sn_x(400)$ set. (b) Linewidth of the brad-band FMR resonance (ΔH) as a function of the microwave frequency. Panels (c,d) show the values of the damping constant, α, and spin mixing conductance, $g_{\uparrow\downarrow}^{eff}$ obtained by using Equations (3) and (4), respectively.

dispersion and the $\Delta H(f_{res})$ curves also for the $Ge_{1-x}Sn_x(400)$. The solid lines indicate the fit based on Equations (2) and (3), respectively. In contrast with the previous findings, M_{eff} turns out to be the same throughout the $Ge_{1-x}Sn_x(400)$ set, with an average value of 1045 ± 6 emu/cm^3 (see Figure S1b, Supporting Information). The latter is very close to 1100–1400 Oe, which is a typical value for bulk Co and indicates the high magneto-structural quality of the evaporated FM.[15,25,26,36] The independence of M_{eff} on the $Ge_{1-x}Sn_x$ substrate can be ascribed to the intertwined effects of (i) the proximity between the adjacent FM and NM affecting the interface SOC properties and (ii) the varying lattice mismatch between Co and the relaxed $Ge_{1-x}Sn_x$ epilayers, which is imparted by the chosen Sn molar fraction. Notably, such mechanisms are absent in the $Ge_{1-x}Sn_x(40)$ series, since the $Ge_{1-x}Sn_x$ epilayers are always grown in full registry with the Ge-buffered Si substrate and because of the presence of the Au interposer between the FM and the NM.

From the dataset shown in Figure 3b, we retrieved the α values reported in panel c of the same figure. Surprisingly, the damping constant and the spin-mixing conductance for $Ge_{1-x}Sn_x(400)$ demonstrate the bell-like dependence peaked at the same Sn molar fraction (~10-11%) observed for $Ge_{1-x}Sn_x(40)$ (see Figure 2c,d).

These findings demonstrate that, under our experimental conditions, Co-GeSn hybridization does not provide sufficient exchange splitting to yield a sizeable spin diffusion out of the NM/FM interface. Above all, the agreement obtained through the SP into the coherent and relaxed $Ge_{1-x}Sn_x$ epitaxial layers (i.e., $Ge_{1-x}Sn_x(40)$ and $Ge_{1-x}Sn_x(400)$, respectively) offers crucial evidence that strain and possibly the direct-to-indirect band gap crossover cannot be regarded as effective mechanisms in governing spin-pumping processes in these novel alloys.

Since nonequilibrium spin accumulation is dissipated in the NM layer by spin-flip processes, we suggest that spin-dependent alloy-induced scattering suffices to describe the observed Sn-related dependence of the magnetization dynamics. In this context, the enhanced Gilbert damping constant reported for $Ge_{0.9}Sn_{0.10}$ corresponds to an enhanced spin-injection rate stemming from an alloy-driven reduction of the spin-flip relaxation time. Nonetheless, a detailed and rigorous theoretical investigation is deemed necessary to scrutinize such a physical picture.

3. Conclusion

By means of SP measurements, the spin accumulation mechanisms in $Ge_{1-x}Sn_x$ thin films grown on Ge-on-Si buffers with different thicknesses and Sn concentrations are investigated. Our approach enables us to isolate the contributions of in-plane strain and alloy-controlled SOC, which otherwise are often entangled in literature reports. When coupled with an Au/Co/Au multilayer, the spin mixing conductance for thin $Ge_{1-x}Sn_x$ films (i.e., 40 nm) showed a clear non-monotonic dependence on the Sn molar fraction. SP findings for thicker $Ge_{1-x}Sn_x$ films (i.e., 400 nm), characterized by strain relaxation, demonstrate a $g_{eff}^{\uparrow\downarrow}$ evolution as a function of the Sn molar fraction that rules out strain compensa-

© 2024 The Author(s). Advanced Quantum Technologies published by Wiley-VCH GmbH

25119044, 0, Downloaded from https://onlinelibrary.wiley.com/doi/10.1002/qute.202400508 by CochraneItalia, Wiley Online Library on [23/12/2024]. See the Terms and Conditions (https://onlinelibrary.wiley.com/terms-and-conditions) on Wiley Online Library for rules of use; OA articles are governed by the applicable Creative Commons License

tion effects. Rather, it can be inferred that spin pumping and spin accumulation are governed by spin-flip relaxation times induced by alloying effects.

Our results represent the first steps toward the investigation of the SCC properties in $Ge_{1-x}Sn_x$ thin films, where the variation of the Sn molar fraction, the different $Ge_{1-x}Sn_x$ layer thickness, and the $Ge_{1-x}Sn_x$/FM interface engineering are exploited to shed some light on the interplay between strain, SOC, and tuning of the band gap character in the studied systems. This manuscript aims to open the path toward the optimization of $Ge_{1-x}Sn_x$-based heterostructures for their future application in spintronics as spin-to-charge interconverters.

4. Experimental Section

$Ge_{1-x}Sn_x$ samples with a thickness of 40 nm were grown on a 100 mm diameter Si(100) substrate. A relaxed Ge buffer layer of ≈650 nm thickness produced a high-quality surface for $Ge_{1-x}Sn_x$ heteroepitaxy, with a root-mean-square surface roughness below 1 nm. The structures were grown using an industrial ASM Epsilon 2000 reduced-pressure chemical vapor deposition reactor with commercially available precursors, digermane (Ge_2H_6) and tin-tetrachloride ($SnCl_4$), diluted in hydrogen. The epitaxial growth was conducted in a hydrogen atmosphere at a reduced pressure below 100 Torr.[37]

$Ge_{1-x}Sn_x$ samples with a thickness of ≈400 nm were deposited on Ge virtual substrates (Ge-VS) on Si(100) wafers through reduced-pressure chemical vapor deposition using an industry-compatible AIXTRON TRICENT reactor. Digermane (Ge_2H_6) and tin tetrachloride ($SnCl_4$) were used as precursors for elementary Ge and Sn, respectively.[13,38,39]

The Co(10 nm)/Au(5 nm) bilayers and Au(5)/Co(10 nm)/Au(5 nm) trilayers were deposited on top of the $Ge_{1-x}Sn_x$ substrates via e-beam evaporation at RT.

The SP-FMR experiments were conducted using a home-made setup, where the sample was positioned between the polar extensions of a Bruker ER-200 electromagnet, maintaining its surface parallel to the external magnetic field (H_{ext}) in the so-called "flip-chip" configuration for in-plane measurements. To induce an oscillating magnetic field in the FM layer, the sample was fixed to a coplanar waveguide connected to a broadband (1–40 GHz) RF-source. The FMR signal for a fixed RF frequency was performed by measuring the derivative of the absorption power downstream of the electrical transmission line as a function of H_{ext} through a lock-in amplifier. For further details on the FMR technique please refer to refs.[25,30,36,40]

Supporting Information

Supporting Information is available from the Wiley Online Library or from the author.

Acknowledgements

The authors express their gratitude to S. Oyarzún and M. Jamet for their insightful discussions. The work was supported financially by the Air Force Office of Scientific Research under award number FA8655-22-1-7050, the PNRR MUR project PE0000023-NQSTI, and the European Commission through the LASTSTEP Project under grant agreement 101070208. Additional funding was provided by the Spanish Ministry of Science and Innovation through Projects PID2023-152225NB-I00 and Severo Ochoa MATRANS42 (CEX2023-001263-S), supported by MICIU/AEI/10.13039/501100011033 and FEDER, EU. The authors also acknowledge support from Projects TED2021-129857B-I00 and PDC2023-145824-I00, funded by MCIN/AEI/10.13039/501100011033 and the European Union NextGeneration EU/PRTR, as well as from project 2021 SGR 00445 funded by the Generalitat de Catalunya.

Conflict of Interest

The authors declare no conflict of interest.

Author Contributions

E.L. conducted the spin pumping experiments and data reduction. O.C., D.B., and M.M. produced the samples and the structural investigations. M.F., R.M., E.B., and J.P. contributed to the data discussion and to the lab activities. F.P. conceived the study and supervised the project. E.L. and F.P. wrote the manuscript with contributions from all the authors.

Data Availability Statement

The data that support the findings of this study are available from the corresponding author upon reasonable request.

Keywords

ferromagnetic resonance, GeSn alloys, spin pumping, spintronics

Received: October 8, 2024
Revised: November 13, 2024
Published online:

[1] N. Jones, *Nature* **2018**, *561*, 163.
[2] J. Sinova, S. O. Valenzuela, J. Wunderlich, C. H. Back, T. Jungwirth, *Rev. Mod. Phys.* **2015**, *87*, 1213.
[3] A. Toriumi, T. Nishimura, *Jpn. J. Appl. Phys.* **2018**, *57*, 010101.
[4] P. S. Goley, M. K. Hudait, *Materials* **2014**, *7*, 2301.
[5] A. Marchionni, C. Zucchetti, F. Ciccacci, M. Finazzi, H. S. Funk, D. Schwarz, M. Oehme, J. Schulze, F. Bottegoni, *Appl. Phys. Lett.* **2021**, *118*, 212402.
[6] B. M. Ferrari, F. Marcantonio, F. Murphy-Armando, M. Virgilio, F. Pezzoli, *Phys. Rev. Res.* **2023**, *5*, L022035.
[7] E. Vitiello, S. Rossi, C. A. Broderick, G. Gravina, A. Balocchi, X. Marie, E. P. O'Reilly, M. Myronov, F. Pezzoli, *Phys. Rev. Appl.* **2020**, *14*, 064068.
[8] S. De Cesari, A. Balocchi, E. Vitiello, P. Jahandar, E. Grilli, T. Amand, X. Marie, M. Myronov, F. Pezzoli, *Phys. Rev. B* **2019**, *99*, 035202.
[9] L. Jin, H. Zhu, D. Zhang, B. Liu, H. Meng, X. Tang, M. Li, Z. Zhong, H. Zhang, *Appl. Phys. Lett.* **2020**, *116*, 122405.
[10] C. Morrison, M. Myronov, *Phys. Status. Solidi. (A) Appl. Mater. Sci.* **2016**, *213*, 2809.
[11] Y. Junk, M. Frauenrath, Y. Han, O. C. Diaz, J. H. Bae, J. M. Hartmann, D. Grutzmacher, D. Buca, Q. T. Zhao, In *European Solid-State Device Research Conference*, Editions Frontieres, Milan, Italy **2022**, pp. 364–367.
[12] D. Buca, A. Bjelajac, D. Spirito, O. Concepción, M. Gromovyi, E. Sakat, X. Lafosse, L. Ferlazzo, N. von den Driesch, Z. Ikonic, D. Grützmacher, G. Capellini, M. El Kurdi, *Adv. Opt. Mater.* **2022**, *10*, 2201024.
[13] O. Concepción, N. B. Søgaard, J. H. Bae, Y. Yamamoto, A. T. Tiedemann, Z. Ikonic, G. Capellini, Q. T. Zhao, D. Grützmacher, D. Buca, *ACS Appl. Electron. Mater.* **2023**, *5*, 2268.
[14] N. von den Driesch, D. Stange, S. Wirths, D. Rainko, I. Povstugar, A. Savenko, U. Breuer, R. Geiger, H. Sigg, Z. Ikonic, J. M. Hartmann, D. Grützmacher, S. Mantl, D. Buca, *Small* **2017**, *13*, 1603321.
[15] M. Farle, *Rep. Prog. Phys.* **1998**, *61*, 755.
[16] M. Tokaç, S. A. Bunyaev, G. N. Kakazei, D. S. Schmool, D. Atkinson, A. T. Hindmarch, *Phys. Rev. Lett.* **2015**, *115*, 056601.

© 2024 The Author(s). Advanced Quantum Technologies published by Wiley-VCH GmbH

25119044, 0, Downloaded from https://onlinelibrary.wiley.com/doi/10.1002/qute.202400508 by CochraneItalia, Wiley Online Library on [23/12/2024]. See the Terms and Conditions (https://onlinelibrary.wiley.com/terms-and-conditions) on Wiley Online Library for rules of use; OA articles are governed by the applicable Creative Commons License

[17] J. M. L. Beaujour, W. Chen, A. D. Kent, J. Z. Sun, *J. Appl. Phys.* **2006**, *99*, 08N503.
[18] S. Kaneta-Takada, M. Yamada, S. Sato, S. Arai, L. D. Anh, K. Hamaya, S. Ohya, *Phys. Rev. Appl.* **2020**, *14*, 024096.
[19] C. Chappert, K. L. Dang, P. Beauvillain, H. Hurdequint, D. Renard, *Phys. Rev. B* **1986**, *34*, 3192.
[20] L. Gladczuk, P. Aleshkevych, K. Lasek, P. Przyslupski, *J. Appl. Phys.* **2014**, *116*, 233909.
[21] P. Ruiz-Díaz, T. R. Dasa, V. S. Stepanyuk, *Phys. Rev. Lett.* **2013**, *110*, 267203.
[22] X. Chen, K. Y. Wang, Z. L. Wu, S. L. Jiang, G. Yang, Y. Liu, J. Teng, G. H. Yu, *Appl. Phys. Lett.* **2014**, *105*, 092402.
[23] A. Wawro, Z. Kurant, L. T. Baczewski, P. Pankowski, J. B. Pełka, A. Maneikis, A. Bójko, V. Zablotskii, A. Maziewski, *physica status solidi c* **2006**, *3*, 77.
[24] P. Beauvillain, C. Chappert, K. L. Dang, R. Mgy, S. O. Mahfoud, P. Veillet, *J. Magn. Magn. Mater.* **1996**, *154*, 160.
[25] E. Longo, M. Belli, M. Alia, M. Rimoldi, R. Cecchini, M. Longo, C. Wiemer, L. Locatelli, P. Tsipas, A. Dimoulas, G. Gubbiotti, M. Fanciulli, R. Mantovan, *Adv. Funct. Mater.* **2021**, *32*, 2109361.
[26] E. Longo, C. Wiemer, M. Belli, R. Cecchini, M. Longo, M. Cantoni, C. Rinaldi, M. D. Overbeek, C. H. Winter, G. Gubbiotti, G. Tallarida, M. Fanciulli, R. Mantovan, *J. Magn. Magn. Mater.* **2020**, *509*, 166885.
[27] S. Dushenko, M. Koike, Y. Ando, T. Shinjo, M. Myronov, M. Shiraishi, *Phys. Rev. Lett.* **2015**, *114*, 196602.
[28] Y. Tserkovnyak, A. Brataas, G. E. W. Bauer, *Phys. Rev. B Condens. Matter Mater. Phys.* **2002**, *66*, 224403.
[29] Y. Tserkovnyak, A. Brataas, G. E. W. Bauer, *Phys. Rev. Lett.* **2002**, *88*, 4.
[30] E. Longo, A. Markou, C. Felser, M. Belli, A. Serafini, P. Targa, D. Codegoni, M. Fanciulli, R. Mantovan, *Adv. Funct. Mater.* **2024**, *34*, 2407968.
[31] J. Bass, W. P. Pratt, *J. Phys.: Condens. Matter* **2007**, *19*, 183201.
[32] S. Wirths, D. Buca, S. Mantl, *Prog. Cryst. Growth Charact. Mater.* **2016**, *62*, 1.
[33] C. T. Tai, P. Y. Chiu, C. Y. Liu, H. S. Kao, C. T. Harris, T. M. Lu, C. T. Hsieh, S. W. Chang, J. Y. Li, *Adv. Mater.* **2021**, *33*, 2007862.
[34] S. Oyarzún, A. K. Nandy, F. Rortais, J. C. Rojas-Sánchez, M. T. Dau, P. Noël, P. Laczkowski, S. Pouget, H. Okuno, L. Vila, C. Vergnaud, C. Beigné, A. Marty, J. P. Attané, S. Gambarelli, J. M. George, H. Jaffrès, S. Blügel, M. Jamet, *Nat. Commun.* **2016**, *7*, 13857.
[35] S. Rossi, E. T. Simola, M. Raimondo, M. Acciarri, J. Pedrini, A. Balocchi, X. Marie, G. Isella, F. Pezzoli, S. Rossi, M. Raimondo, J. Pedrini, F. Pezzoli, E. T. Simola, G. Isella, A. Balocchi, X. Marie, *Adv. Opt. Mater.* **2022**, *10*, 2201082.
[36] E. Longo, L. Locatelli, M. Belli, M. Alia, A. Kumar, M. Longo, M. Fanciulli, R. Mantovan, *Adv. Mater. Interfaces* **2021**, *2101244*, 2101244.
[37] F. Pezzoli, A. Giorgioni, D. Patchett, M. Myronov, *ACS Photonics* **2016**, *3*, 2004.
[38] N. Von Den Driesch, D. Stange, S. Wirths, G. Mussler, B. Holländer, Z. Ikonic, J. M. Hartmann, T. Stoica, S. Mantl, D. Grützmacher, D. Buca, *Chem. Mater.* **2015**, *27*, 4693.
[39] D. Stange, S. Wirths, R. Geiger, C. Schulte-Braucks, B. Marzban, N. V. Den Driesch, G. Mussler, T. Zabel, T. Stoica, J. M. Hartmann, S. Mantl, Z. Ikonic, D. Grützmacher, H. Sigg, J. Witzens, D. Buca, *ACS Photonics* **2016**, *3*, 1279.
[40] E. Georgopoulou-Kotsaki, P. Pappas, A. Lintzeris, P. Tsipas, S. Fragkos, A. Markou, C. Felser, E. Longo, M. Fanciulli, R. Mantovan, F. Mahfouzi, N. Kioussis, A. Dimoulas, *Nanoscale* **2023**, *15*, 2223.

© 2024 The Author(s). Advanced Quantum Technologies published by Wiley-VCH GmbH

25119044, 0, Downloaded from https://onlinelibrary.wiley.com/doi/10.1002/qute.202400508 by CochraneItalia, Wiley Online Library on [23/12/2024]. See the Terms and Conditions (https://onlinelibrary.wiley.com/terms-and-conditions) on Wiley Online Library for rules of use; OA articles are governed by the applicable Creative Commons License